

X-RAY DIFFRACTION RESIDUAL STRESS TECHNIQUES

Paul S. Prevéy, Lambda Research, Inc.

GENERAL USES

Macrostress measurement

- Nondestructive surface residual stress measurement for quality control.
- Determination of subsurface residual stress distributions
- Measurement of residual stresses associated with failures caused by fatigue or stress corrosion

Microstress measurement

- Determination of the percent cold work at and below the surface
- Measurement of hardness in steels in thin layers

EXAMPLES OF APPLICATIONS

- Determination of the depth and magnitude of the compressive layer and hardness produced by carburizing steels
- Investigation of the uniformity of the surface compressive residual stresses produced by shot peening in complex geometries
- Measurement of surface residual stresses and hardness on the raceway of ball and roller bearings as functions of the hours of service
- Study of the alteration of residual stress and percent cold work distributions caused by stress-relieving heat treatment or forming
- Measurement of surface and subsurface residual stresses parallel and perpendicular to a weld fusion line as a function of distance from the weld
- Determination of the direction of maximum residual stress and percent cold work gradient caused by machining

SAMPLES

- *Form:* Polycrystalline solids, metallic or ceramic, moderate to fine grained
- *Size:* Various, with limitations dictated by the type of apparatus, the stress field to be examined, and x-ray optics
- *Preparation:* Generally, none. Large samples and inaccessible areas may require sectioning with prior strain gaging to record the resulting stress relaxation. Careful handling or protective coatings may be required to preserve surface stresses

LIMITATIONS

- Expensive, delicate apparatus generally limited to a laboratory or shop
- Only shallow (<0.025 mm, or 0.001 in.) surface layer is measured, requiring electrolytic polishing to remove layers for subsurface measurement
- Samples must be polycrystalline, of reasonably fine grain size, and not severely textured

ESTIMATED ANALYSIS TIME

- 1 min. to 1 hr. per measurement, depending on the diffracted x-ray intensity and technique used. Typically, 1 hr. per measurement for subsurface work, including material removal and sample repositioning

CAPABILITIES OF RELATED TECHNIQUES

- *General dissection techniques:* Generally good for determination of gross residual stress distributions extending over large distances or depths. Restricted to simple geometries
- *Hole drilling:* Applicable to a variety of samples with stress fields uniform over dimensions larger than the strain-gage rosette and depth of the drilled hole and with magnitudes less than nominally 60% of yield strength. Serious errors are possible due to local yielding for higher stresses, variation in the stress field beneath the rosettes, eccentricity of the hole, or as a result of residual stresses induced in drilling the holes.
- *Ultrasonic methods:* Require relatively long gage lengths and stress-free reference standards. Of limited practical application due to errors caused by transducer coupling, preferred orientation, cold work, temperature, and grain size. Sensitivity varies greatly with material.
- *Magnetic (Barkhausen or magnetostrictive) methods:* Limited to ferromagnetic materials and subject to many of the limitations and error sources of ultrasonic methods. Highly nonlinear response with low sensitivity to tensile stresses.

Prevéy, Paul S. "X-ray Diffraction Residual Stress Techniques,"
Metals Handbook. 10. Metals Park: American Society for Metals, 1986, 380-392.

X-RAY DIFFRACTION RESIDUAL STRESS TECHNIQUES

Paul S. Prevéy
Lambda Research

INTRODUCTION

In x-ray diffraction residual stress measurement, the strain in the crystal lattice is measured, and the residual stress producing the strain is calculated, assuming a linear elastic distortion of the crystal lattice. Although the term stress measurement has come into common usage, stress is an extrinsic property that is not directly measurable. All methods of stress determination require measurement of some intrinsic property, such as strain or force and area, and the calculation of the associated stress.

Mechanical methods (dissection techniques) and nonlinear elastic methods (ultrasonic and magnetic techniques) are limited in their applicability to residual stress determination. Mechanical methods are limited by assumptions concerning the nature of the residual stress field and sample geometry. Mechanical methods, being necessarily destructive, cannot be directly checked by repeat measurement. Spatial and depth resolution are orders of magnitude less than those of x-ray diffraction.

All nonlinear elastic methods are subject to major error from preferred orientation, cold work, temperature, and grain size. All require stress-free reference samples, which are otherwise identical to the sample under investigation. Nonlinear elastic methods are generally not suitable for routine residual stress determination at their current state of development. In addition, their spatial and depth resolutions are orders of magnitude less than those of x-ray diffraction.

To determine the stress, the strain in the crystal lattice must be measured for at least two precisely known orientations relative to the sample surface. Therefore, x-ray diffraction residual stress measurement is applicable to materials that are crystalline, relatively fine grained, and produce diffraction for any orientation of the sample surface. Samples may be metallic or ceramic, provided a diffraction peak of suitable intensity and free of interference from neighboring peaks can be produced in the high back-reflection region with the radiations available. X-ray diffraction residual stress measurement is

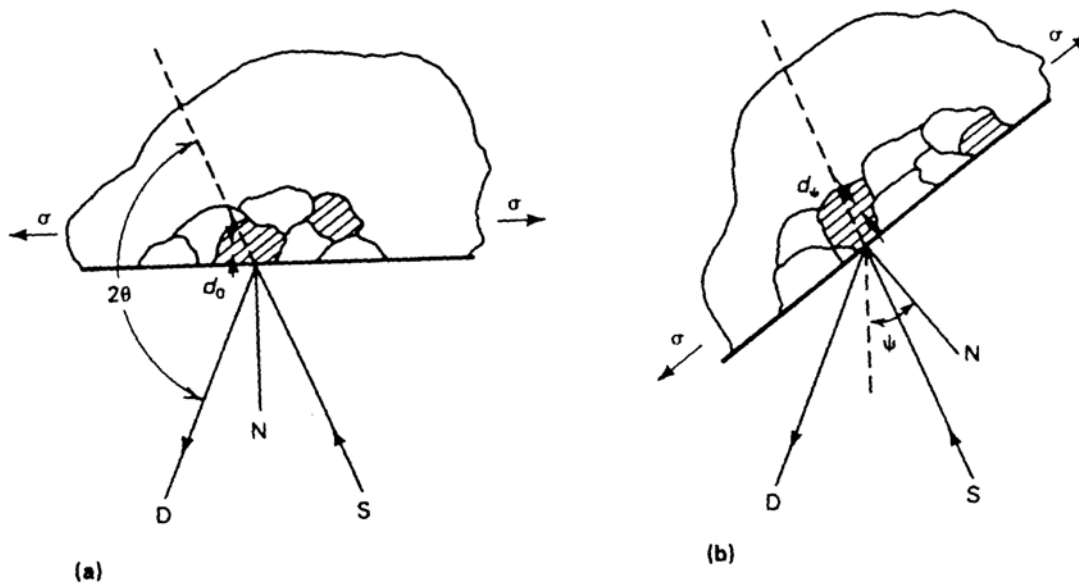
unique in that macroscopic and microscopic residual stresses can be determined nondestructively.

Macroscopic stresses, or macrostresses, which extend over distances that are large relative to the grain size of the material, are of general interest in design and failure analysis. Macrostresses are tensor quantities, with magnitudes varying with direction at a single point in a body. The macrostress for a given location and direction is determined by measuring the strain in that direction at a single point. When macrostresses are determined in at least three known directions, and a condition of plane stress is assumed, the three stresses can be combined using Mohr's circle for stress to determine the maximum and minimum residual stresses, the maximum shear stress, and their orientation relative to a reference direction. Macrostresses strain many crystals uniformly in the surface. This uniform distortion of the crystal lattice shifts the angular position of the diffraction peak selected for residual stress measurement.

Microscopic stresses, or microstresses, are scalar properties of the sample, such as percent of cold work or hardness, that are without direction and result from imperfections in the crystal lattice. Microstresses are associated with strains within the crystal lattice that traverse distances on the order of or less than the dimensions of the crystals. Microstresses vary from point to point within the crystal lattice, altering the lattice spacing and broadening the diffraction peak. Macrostresses and microstresses can be determined separately from the diffraction peak position and breadth.

Principles of X-Ray Diffraction Stress Measurement

Figure 1 shows the diffraction of a monochromatic beam of x-rays at a high diffraction angle (2θ) from the surface of a stressed sample for two orientations of the sample relative to the x-ray beam. The angle ψ , defining the orientation of the sample surface, is the angle between the normal of the surface and the incident and diffracted beam bisector, which is also the angle between the normal to the diffracting lattice planes and the sample surface.



(a) $\psi = 0$. (b) $\psi = \psi$ (sample rotated through some known angle ψ). D, x-ray detector; S, x-ray source; N, normal to the surface.

Fig. 1 -Principles of x-ray diffraction stress measurement.

Diffraction occurs at an angle 2θ , defined by Bragg's Law: $n\lambda = 2d \sin \theta$, where n is an integer denoting the order of diffraction, λ is the x-ray wavelength, d is the lattice spacing of crystal planes, and θ is the diffraction angle. For the monochromatic x-rays produced by the metallic target of an x-ray tube, the wavelength is known to 1 part in 10^5 . Any change in the lattice spacing, d , results in a corresponding shift in the diffraction angle 2θ .

Figure 1 (a) shows the sample in the $\psi = 0$ orientation. The presence of a tensile stress in the sample results in a Poisson's ratio contraction, reducing the lattice spacing and slightly increasing the diffraction angle, 2θ . If the sample is then rotated through some known angle ψ (Fig. 1b), the tensile stress present in the surface increases the lattice spacing over the stress-free state and decreases 2θ . Measuring the change in the angular position of the diffraction peak for at least two orientations of the sample defined by the angle ψ enables calculation of the stress present in the sample surface lying in the plane of diffraction, which contains the incident and diffracted x-ray beams. To measure the stress in different directions at the same point, the sample is rotated about its surface normal to coincide the direction of interest with the diffraction plane.

Because only the elastic strain changes the mean lattice spacing, only elastic strains are measured using x-ray diffraction for the determination of macrostresses. When the elastic limit is exceeded, further strain results in dislocation motion, disruption of the crystal lattice, and the formation of microstresses, but no additional increase in macroscopic stress. Although residual stresses result from nonuniform plastic deformation, all residual

macrostresses remaining after deformation are necessarily elastic.

The residual stress determined using x-ray diffraction is the arithmetic average stress in a volume of material defined by the irradiated area, which may vary from square centimeters to square millimeters, and the depth of penetration of the x-ray beam. The linear absorption coefficient of the material for the radiation used governs the depth of penetration, which can vary considerably. However, in iron, nickel, and aluminum-base alloys, 50% of the radiation is diffracted from a layer approximately 0.005 mm (0.0002 in.) deep for the radiations generally used for stress measurement. This shallow depth of penetration allows determination of macro and microscopic residual stresses as functions of depth, with depth resolution approximately 10 to 100 times that possible using other methods.

Although in principle virtually any interplanar spacing may be used to measure strain in the crystal lattice, availability of the wavelengths produced by commercial x-ray tubes limits the choice to a few possible planes. The choice of a diffraction peak selected for residual stress measurement impacts significantly on the precision of the method. The higher the diffraction angle, the greater the precision. Practical techniques generally require diffraction angles, 2θ , greater than 120° .

Table I lists recommended diffraction techniques for various alloys. The relative sensitivity is shown by the value of K_{45} , the magnitude of the stress necessary to cause an apparent shift in diffraction-peak position of 1° for a $45^\circ\psi$ tilt. As K_{45} increases, sensitivity decreases.

Table I Recommended diffraction techniques, x-ray elastic constants, and bulk values for various ferrous and nonferrous alloys

Alloy	Radiation	Lattice		Elastic constants(a) ($E/1 = \nu$)					Linear	
		plane, angle	(hkl)	GPa (10^6 psi)		Bulk		Absorption		
		(2θ), degrees		Bulk	Error %	$K_{45}(b)$	Coefficient (μ)			
							MPa	ksi	cm^{-1}	$in.^{-1}$
Aluminum-base alloys										
2014-T6	Cr $K\alpha$	(311)	139.0	59.4 ± 0.76 (8.62 ± 0.11)	54.5 (7.9)	-8.3	387	56.2	442	1124
2024-T351	Cr $K\alpha$	(311)	139.3	53.8 ± 0.55 (7.81 ± 0.08)	54.5 (7.9)	+1.1	348	50.5	435	1105
7075-T6	Cr $K\alpha$	(311)	139.0	$60.9 \pm .048$ (8.83 ± 0.07)	53.8 (7.8)	-11.4	397	57.6
7050-T6	Cr $K\alpha$	(311)	139.0	57.1 ± 0.41 (8.28 ± 0.06)	53.8 (7.8)	-5.8	372	54.0	443	1126
Iron-base alloys										
Incoloy 800	Cu $K\alpha$	(420)	147.2	148.2 ± 2.8 (21.5 ± 0.4)	147.5 (21.4)	-0.4	758	110.0	1656	4205
304L	Cu $K\alpha$	(420)	147.0	157.2 ± 2.8 (22.8 ± 0.4)	151.0 (21.9)	-3.9	814	118.0	2096	5321
316	Cu $K\alpha$	(420)	146.5	132.4 ± 1.4 (19.2 ± 0.2)	153.8 (22.3)	+16.0	696	101.0	2066	5245
Invar	Cu $K\alpha$	(420)	147.0	108.2 ± 4.1 (15.7 ± 0.6)	112.4 (16.3)	+3.8	560	81.2	1706	4330
410 (22 HRC)	Cr $K\alpha$	(211)	155.1	176.5 ± 0.7 (25.6 ± 0.1)	155.8 (22.6)	-11.7	680	98.6	840	2129
410 (42 HRC)	Cr $K\alpha$	(211)	155.1	173.1 ± 1.4 (25.1 ± 0.2)	155.8 (22.6)	-9.9	667	96.7	840	2129
1050 (56 HRC)	Cr $K\alpha$	(211)	156.0	184.1 ± 2.1 (26.7 ± 0.3)	148.2 (21.5)	-19.4	683	99.0	885	2244
4340 (50 HRC)	Cr $K\alpha$	(211)	156.0	168.9 ± 2.8 (24.5 ± 0.4)	156.5 (22.7)	-7.3	627	90.9	909	2307
6260	Cr $K\alpha$	(211)	155.5	169.6 ± 2.8 (24.6 ± 0.4)	158.9 (23.0)	-6.5	643	93.2	894	2271
9310	Cr $K\alpha$	(211)	155.5	172.4 ± 2.8 (25.0 ± 0.4)	160.0 (23.2)	-7.2	653	94.7	894	2271
52100	Cr $K\alpha$	(211)	156.0	173.7 ± 2.1 (25.2 ± 0.3)	153.8 (22.3)	-11.5	645	93.5	714	1807
M50 (62 HRC)	Cr $K\alpha$	(211)	154.0	179.3 ± 2.1 (26.0 ± 0.3)	157.9 (22.9)	-11.9	724	105.0	1000	2490
17-4PH	Cr $K\alpha$	(211)	155.0	180.0 ± 0.7 (26.1 ± 0.1)	158.9 (23.0)	-11.9	696	101.0	888	2254
Nickel-base alloys										
Inconel 600	Cu $K\alpha$	(420)	150.8	159.3 ± 0.7 (23.1 ± 0.1)	165.5 (24.0)	+3.9	724	105.0	896	2275
Inconel 718	Cu $K\alpha$	(420)	145.0	140.0 ± 2.1 (20.3 ± 0.3)	156.5 (22.7)	-8.9	772	112.0	1232	3127
Inconel X-750	Cu $K\alpha$	(420)	151.0	160.6 ± 1.4 (23.3 ± 0.2)	160.6 (24.0)	+3.0	724	105.0	813	2062
Incoloy 901	Cu $K\alpha$	(420)	146.0	134.4 ± 3.4 (19.5 ± 0.5)	158.6 (23.0)	+17.9	717	104.0	1408	3569
Rene 95	Cu $K\alpha$	(420)	146.7	168.9 ± 0.7 (24.5 ± 0.1)	164.1 (23.8)	-2.8	882	128.0	935	2370
Titanium-base alloys										
Commercially pure Ti	Cu $K\alpha$	(21.3)	139.5	90.3 ± 1.4 (13.1 ± 0.2)	84.8 (12.3)	-6.1	581	84.3	917	2320
Ti-6Al-4V	Cu $K\alpha$	(21.3)	141.7	84.1 ± 0.7 (12.2 ± 0.1)	84.8 (12.3)	+0.8	509	73.9	867	2203
Ti-6Al-2Sn-4Zr-2Mo	Cu $K\alpha$	(21.3)	141.5	102.0 ± 1.4 (14.8 ± 0.2)	86.2 (12.5)	-15.5	622	90.2	866	2200

(a) Constants determined from four-point bending tests. (b) K_{45} is the magnitude of the stress necessary to cause an apparent shift in diffraction-peak position of 1° for 45° angle tilt

Plane-Stress Elastic Model

X-ray diffraction stress measurement is confined to the surface of the sample. Electropolishing is used to expose new surfaces for subsurface measurement. In the exposed surface layer, a condition of plane stress is assumed to exist. That is, a stress distribution described by principal

stresses σ_1 and σ_2 exists in the plane of the surface, and no stress is assumed perpendicular to the surface, $\sigma_3 = 0$. However, a strain component perpendicular to the surface ϵ_3 exists as a result of the Poisson's ratio contractions caused by the two principal stresses (Fig. 2).

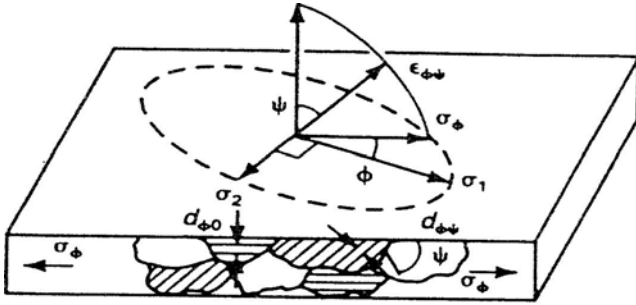


Fig. 2 -Plane-stress elastic model

The strain, $\epsilon_{\phi\psi}$ in the direction defined by the angles ϕ and ψ is:

$$\epsilon_{\phi\psi} = \left[\frac{1+\nu}{E} (\sigma_1 \alpha_1^2 + \sigma_2 \alpha_2^2) \right] - \left[\frac{\nu}{E} (\sigma_1 + \sigma_2) \right] \tag{Eq 1}$$

where E is the modulus of elasticity, ν is the Poisson's ratio, and α_1 and α_2 are the angle cosines of the strain vector:

$$\begin{aligned} \alpha_1 &= \cos\phi \sin\psi \\ \alpha_2 &= \sin\phi \sin\psi \end{aligned} \tag{Eq 2}$$

Substituting for the angle cosines in Eq 1 and simplifying enables expressing the strain in terms of the orientation angles:

$$\epsilon_{\phi\psi} = \left[\frac{1+\nu}{E} (\sigma_1 \cos^2\phi + \sigma_2 \sin^2\phi) \sin^2\psi \right] - \left[\frac{\nu}{E} (\sigma_1 + \sigma_2) \right] \tag{Eq 3}$$

If the angle ψ is taken to be 90° , the strain vector lies in the plane of the surface, and the surface stress component, σ_ϕ is:

$$\sigma_\phi = (\sigma_1 \cos^2\phi) + (\sigma_2 \sin^2\phi) \tag{Eq 4}$$

Substituting Eq 4 into Eq 3 yields the strain in the sample surface at an angle ϕ from the principal stress σ_1 :

$$\epsilon_{\phi\psi} = \left[\frac{1+\nu}{E} \sigma_\phi \sin^2\psi \right] - \left[\left(\frac{\nu}{E} \right) (\sigma_1 + \sigma_2) \right] \tag{Eq 5}$$

Equation 5 relates the surface stress σ_ϕ , in any direction defined by the angle ψ , to the strain, ϵ , in the direction (ϕ, ψ) and the principal stresses in the surface.

If $d_{\phi\psi}$ is the spacing between the lattice planes measured in the direction defined by ϕ and ψ , the strain can be expressed in terms of changes in the linear dimensions of the crystal lattice:

$$\epsilon_{\phi\psi} = \frac{\Delta d}{d_0} = \frac{d_{\phi\psi} - d_0}{d_0}$$

where d_0 is the stress-free lattice spacing. Substitution into Eq 5 yields:

$$\begin{aligned} \frac{d_{\phi\psi} - d_0}{d_0} &= \left[\left(\frac{1+\nu}{E} \right)_{(hkl)} \sigma_\phi \sin^2\psi \right] - \\ &\left[\left(\frac{\nu}{E} \right)_{(hkl)} (\sigma_1 + \sigma_2) \right] \end{aligned} \tag{Eq 6}$$

where the elastic constants $(1 + \nu/E)_{(hkl)}$ and $(\nu/E)_{(hkl)}$ are not the bulk values but the values for the crystallographic direction normal to the lattice planes in which the strain is measured as specified by the Miller indices (hkl) . Because of elastic anisotropy, the elastic constants in the (hkl) direction commonly vary significantly from the bulk mechanical values, which are an average over all possible directions in the crystal lattice.

The lattice spacing for any orientation, then, is:

$$\begin{aligned} d_{\phi\psi} &= \left[\left(\frac{1+\nu}{E} \right)_{(hkl)} \sigma_\phi d_0 \sin^2\psi \right] - \\ &\left[\left(\frac{\nu}{E} \right)_{(hkl)} d_0 (\sigma_1 + \sigma_2) + d_0 \right] \end{aligned} \tag{Eq 7}$$

Equation 7 describes the fundamental relationship between lattice spacing and the biaxial stresses in the surface of the sample. The lattice spacing $d_{\phi\psi}$, is a linear function of $\sin^2\psi$. Figure 3 shows the actual dependence of $d(311)$ for ψ , ranging from 0 to 45° for shot peened 5056-O aluminum having a surface stress of -148 MPa (-21.5 ksi), to which a straight line has been fitted by least squares regression.

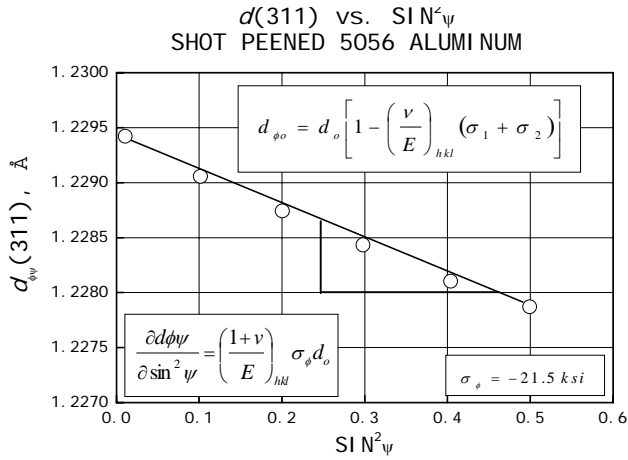


Fig. 3 - A $d(311)$ versus $\sin^2\psi$ plot for a shot peened 5056-O aluminum alloy having a surface stress of -148 MPa (-21.5 ksi)

The intercept of the plot at $\sin^2\psi = 0$ is:

$$d_{\phi 0} = d_0 - \left(\frac{\nu}{E}\right)_{(hkl)} d_0(\sigma_1 + \sigma_2) = d_0 \left[1 - \left(\frac{\nu}{E}\right)_{(hkl)} (\sigma_1 + \sigma_2) \right]$$

Eq 8)

which equals the unstressed lattice spacing, d_0 , minus the Poisson's ratio contraction caused by the sum of the principal stresses. The slope of the plot is:

$$\frac{\partial d_{\phi\psi}}{\partial \sin^2\psi} = \left(\frac{1+\nu}{E}\right)_{(hkl)} \sigma_{\phi} d_0$$

which can be solved for the stress σ_{ϕ} :

$$\sigma_{\phi} = \left(\frac{E}{1+\nu}\right)_{(hkl)} \frac{1}{d_{\phi 0}} \left(\frac{\partial d_{\phi\psi}}{\partial \sin^2\psi}\right)$$

(Eq 9)

The x-ray elastic constants can be determined empirically, but the unstressed lattice spacing, d_0 , is generally unknown. However, because $E \gg (\sigma_1 + \sigma_2)$, the value of $d_{\phi 0}$ from Eq 8 differs from d_0 by not more than $\pm 1\%$, and σ_{ϕ} may be approximated to this accuracy using:

$$\sigma_{\phi} = \left(\frac{E}{1+\nu}\right)_{(hkl)} \frac{1}{d_{\phi 0}} \left(\frac{\partial d_{\phi\psi}}{\partial \sin^2\psi}\right)$$

(Eq 10)

The method then becomes a differential technique, and no stress-free reference standards are required to determine d_0 for the biaxial stress case. The three most common methods of x-ray diffraction residual stress measurement, the single-angle, two-angle, and $\sin^2\psi$ techniques, assume plane stress at the sample surface and are based on the fundamental relationship between lattice spacing and stress given in Eq 7.

The single-angle technique, or single-exposure technique, derives its name from early photographic methods that require a single exposure of the film (Ref 1).

The method is generally considered less sensitive than the two-angle or $\sin^2\psi$ techniques primarily because the possible range of ψ is limited by the diffraction angle 2θ .

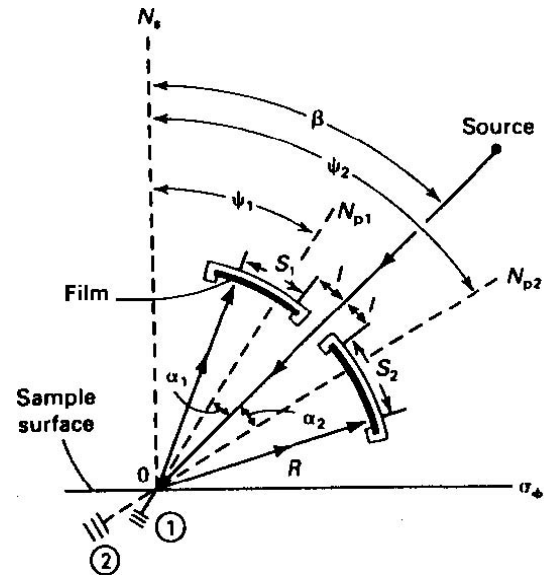


Fig. 4 - Basic geometry of the single-angle technique for x-ray diffraction residual stress measurement N_p , normal to the lattice planes; N_s , normal to the surface. See text for a discussion of other symbols. Source: Ref 2

Figure 4 shows the basic geometry of the method. A collimated beam of x-rays is inclined at a known angle, β , from the sample surface normal. X-rays diffract from the sample, forming a cone of diffracted radiation originating at point 0. The diffracted x-rays are recorded using film or position-sensitive detectors placed on either side of the incident beam. The presence of a stress in the sample surface varies the lattice spacing slightly between the diffracting crystals shown at points 1 and 2 in Fig. 4, resulting in slightly different diffraction angles on either side of the x-ray beam. If S_1 , and S_2 are the arc lengths along the surface of the film or detectors at a radius R from the sample surface, the stress is:

$$\sigma_{\phi} = \left(\frac{E}{1+\nu}\right)_{(hkl)} \left(\frac{s_1 - s_2}{2R}\right) \left(\frac{\cot\theta}{\sin^2\psi_1 - \sin^2\psi_2}\right)$$

The angles ψ_1 , and ψ_2 are related to the Bragg diffraction angles θ_1 , θ_2 , and the angle of inclination of the instrument, β , by:

$$\psi_1 = \beta + \theta_1 - \frac{\pi}{2}$$

and

$$\psi_2 = \beta + \theta_2 - \frac{\pi}{2}$$

The precision of the method is limited by the principle that increasing the diffraction angle 2θ to achieve precision in the determination of lattice spacing reduces the possible range of $\sin^2\psi$, lessening sensitivity. The single-angle technique is generally not used, except for film and position-sensitive detector apparatuses designed for high-speed measurement.

Two-Angle Technique. Equation 7 and Fig. 3 show that if the lattice spacing, d_{ψ} is a linear function of $\sin^2\psi$, the stress can be determined by measuring the lattice spacing for any two ψ angles, originating the term two-angle technique. The technique has been thoroughly investigated by the Society of Automotive Engineers (SAE) and finds wide acceptance in the United States (Ref 3). Selecting ψ angles to provide as large a range of $\sin^2\psi$ as possible within the limitations imposed by the diffraction angle 2θ and the sample geometry maximizes sensitivity of the method. Lattice spacing is determined precisely at two extreme values of ψ , typically 0 and 45°, and the stress is calculated using Eq 10.

The $\sin^2\psi$ technique (Ref 4) is identical to the two-angle technique, except lattice spacing is determined for multiple ψ tilts, a straight line is fitted by least squares regression (as shown for the shot peened aluminum sample in Fig. 3), and the stress is calculated from the slope of the best fit line using Eq 10. The method, a standard procedure in Japan and Germany, provides no significant improvement in precision over the two-angle technique if the two data points are selected at the extreme ends of the $\sin^2\psi$ range.

The primary advantage of the $\sin^2\psi$ technique, considering the additional time required for data collection, is in establishing the linearity of d as a function of $\sin^2\psi$ to demonstrate that x-ray diffraction residual stress measurement is possible on the sample of interest.

The Marion-Cohen technique characterizes the dependence of lattice spacing on stress in highly textured materials (Ref 5). The method assumes a biaxial stress field with an additional dependence of the lattice spacing on a texture distribution function $f(\psi)$, a measure of the (hkl) pole density calculated from the diffracted intensity

over the range of ψ tilts used for stress measurement. The model assumes a lattice spacing dependence of:

$$d_{\psi\phi} = \left(\frac{1+\nu}{E} \right)_{(hkl)} \sigma_{\phi} d_0 \sin^2 \psi + (d_{\max} - d_B) f(\psi) + d_B$$

where d_{\max} and d_B are the maximum and minimum lattice spacings in the range investigated. The method requires simultaneous determination of the preferred orientation, or texture, in the sample to determine $f(\psi)$ along with lattice spacing and is solved by multiple linear regression over the functions $f(\psi)$ and $d_{\psi\phi}$ as functions of $\sin^2\psi$ to determine σ_{ϕ} , d_{\max} , and d_B .

The assumption that the lattice spacing and preferred orientation present at the time of measurement resulted entirely from the same origin limits practical application of the method. Residual stresses measured by the Marion-Cohen, two-angle, and $\sin^2\psi$ methods yield virtually identical results for stress produced by shot peening, grinding, or machining in most materials of practical interest (Ref 6).

Full-Tensor Determination. An expression for the lattice spacing can be formulated as a function of ϕ and ψ , assuming stresses exist normal to the surface. This state of stress in the surface layers penetrated by the x-ray beam is a possible explanation for nonlinear dependence of the lattice spacing on $\sin^2\psi$. Nonlinearities in the form of elliptical curvature of the $d \sin^2\psi$ plots resulting in ψ splitting are attributable to stresses normal to the surface or large shear stresses near the sample surface. ψ splitting results in different values of the lattice spacing for positive and negative ψ tilts and potential error in stress calculation.

In principle, the full-tensor method (Ref 7, 8) can be used to determine surface stresses nondestructively in the presence of large subsurface stress gradients, such as those found on machined or ground samples; however, extensive data collection is required, generally exceeding that acceptable for routine testing. Unlike the plane-stress methods, determination of the full stress tensor requires absolute knowledge of the unstressed lattice spacing, d_0 , at the accuracy required for strain measurement (1 part in 10^5) to calculate the stress normal to the sample surface. In many cases, such as for plastically deformed surfaces generated by machining or carburized steels, the lattice spacing varies as a result of deformation or heat treating, precluding independent determination of the unstressed lattice spacing with sufficient precision. The extensive data collection and dependence on absolute knowledge of d_0 limit the full-tensor method primarily to research applications. If measurements can be performed destructively, by electropolishing to remove layers, surface results obtained using the plane-stress method can

be corrected for the presence of the subsurface stress gradient (Ref 9).

BASIC PROCEDURE

Sample preparation, if the geometry of the sample does not interfere with the incident or diffracted x-ray beams, is generally minimal. Preparation of the sample surface depends on the nature of the residual stresses to be determined. If the stresses of interest are produced by such surface treatments as machining, grinding, or shot peening, the residual stress distribution is usually limited to less than 500 μm of the sample surface. Therefore, the sample surface must be carefully protected from secondary abrasion, corrosion, or etching. Samples should be oiled to prevent corrosion and packed to protect the surface during handling. Secondary abrasive treatment, such as wire brushing or sand blasting, radically alters the surface residual stresses, generally producing a shallow, highly compressive layer over the original residual stress distribution.

If the stresses of interest are those produced by carburizing or heat treatment, it may be advisable to electropolish the surface of the sample, which may have undergone finish grinding or sand blasting after heat treatment. Electropolishing eliminates the shallow, highly stressed surface layer, exposing the subsurface stresses before measurement.

To measure the inside surface of tubing, in bolt holes, between gear teeth, and other restrictive geometries, the sample must be sectioned to provide clearance for the incident and diffracted x-ray beams. Unless prior experience with the sample under investigation indicates that no significant stress relaxation occurs upon sectioning, electrical resistance strain-gage rosettes should be applied to the measurement area to record the strain relaxation that occurs during sectioning. Unless the geometry of the sample clearly defines the minimum and maximum directions of stress relaxation, a full rectangular strain-gage rosette should be used to calculate the true stress relaxation in the direction of interest from the measured strain relaxation.

Following x-ray diffraction residual stress measurements, the total stress before sectioning can be calculated by subtracting algebraically the sectioning stress relaxation from the x-ray diffraction results. If only near-surface layers are examined on a massive sample, a constant relaxation correction can be applied to all depths examined. If a significant volume of material is removed, as in determination of the stress distribution through the carburized case of a thin bearing race, a more accurate representation of sectioning relaxation can be achieved by applying strain-gage rosettes to the inner and outer surfaces and by assuming a linear relaxation of stress through the sample.

Sample Positioning. Because the diffraction angles must be determined to accuracies of approximately $\pm 0.01^\circ$, the sample must be positioned in the x-ray beam at the true center of rotation of the ψ and 2θ axes, and the angle ψ must be constant throughout the irradiated area. Therefore, extremely precise positioning of the sample to accuracies of approximately 0.025 mm (0.001 in.) is critical. Further, the size of the irradiated area must be limited to an essentially flat region on the sample surface. Small diameter samples or such sample geometries as small-radius fillets, the roots of threads, and fine-pitched gears may contribute to major sources of error if the x-ray beam is not confined to an essentially flat region at a known ψ tilt on the curved surface. If the irradiated area is allowed to span a curved surface, ψ will not be constant during determination of lattice spacing. These restrictions imposed by the sample geometry may prohibit x-ray diffraction residual stress measurement in many areas of primary concern, such as the roots of notches.

Irradiated Area and Measurement Time. The residual stress determined by x-ray diffraction is the arithmetic average stress in the area defined by the dimensions of the x-ray beam. Consideration must be given to an appropriate beam size for the nature of the stress to be investigated. If average stresses over significant areas are of interest, the maximum beam size allowed by the geometry of the sample would be an appropriate choice. If local variations in residual stress, such as those produced by individual passes of a grinding wheel, are of interest, a smaller irradiated area with a geometry appropriate for the investigation should be selected. Practical dimensions of the irradiated area may range from circular zones 1.25 mm (0.050 in.) in diameter to a range of rectangular geometries from approximately 0.5 to 13 mm (0.020 to 0.5 in.). The maximum irradiated area generally feasible is approximately 13 x 8 mm (0.5 x 0.3 in.).

As the irradiated area is increased, the data collection time necessary to achieve adequate precision for residual stress measurement diminishes. The precision with which the diffracted intensity can be determined varies as the inverse of the square root of the number of x-rays collected. To determine the intensity to an accuracy of 1% at a single point on the diffraction peak, 10^4 x-rays must be counted, regardless of the time required. With diffracted intensities typically available on a fixed slit diffractometer system, this may require collection times of approximately 30 s for each point on the diffraction peak. If seven data points are collected on each diffraction peak for a two-angle technique, total measurement time may be 10 to 15 min. Reducing the irradiated area sufficiently to decrease the diffracted intensity by an order of magnitude increases the data collection time proportionally for the same precision in measurement. If fluorescence is not a problem, position-sensitive detectors can be used to collect data simultaneously at numerous points across the diffraction peak, with some sacrifice in

angular precision, reducing data collection time by an order of magnitude.

Diffraction-Peak Location. The transition metal target x-ray tubes used for stress measurement produce a continuous spectrum of white radiation and three monochromatic high-intensity lines. The three lines are the $K\alpha_1$, $K\alpha_2$, and $K\beta$ characteristic radiations with wavelengths known to high precision. The $K\alpha_1$ and $K\alpha_2$ lines differ too little in wavelength to allow separation of the diffraction peaks produced. The $K\alpha_1$ line, the highest intensity, is nominally twice that of the $K\alpha_2$ line. The $K\beta$ line is produced at a substantially shorter wavelength and can generally be separated from the $K\alpha$ lines by filtration, the use of high-energy resolution detectors, or crystal monochromators. The $K\beta$ line is typically one fifth the intensity of the $K\alpha_1$ line and is generally too weak for practical x-ray diffraction residual stress measurement on plastically deformed surfaces.

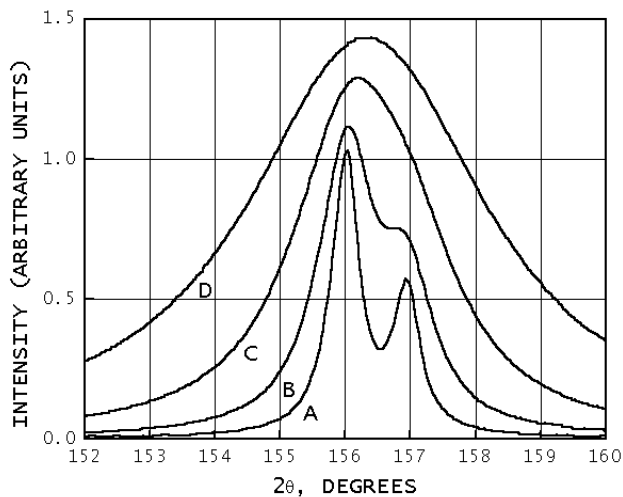


Fig. 5 -Range of $K\alpha$ doublet blending for a simulated steel (211) Cr $K\alpha$ peak at 156.0° . A, fully annealed, B and C, intermediate hardness; D, fully hardened

Because the $K\alpha$ doublet is generally used for residual stress measurement, the diffraction peaks produced consist of a superimposed pair of peaks, as shown in Fig. 5 for four cases, indicating the various degrees of broadening that may be encountered. The variable blending of the $K\alpha$ doublet typical of an annealed sample is indicated by curve A; a fully hardened or cold-worked sample, curve D. Because the accuracy of x-ray diffraction residual stress measurement depends on the precision with which the diffraction peak can be located, the method used to locate broadened doublet peaks is of primary importance.

Precise determination of the position of the diffraction peak at each ψ tilt begins with collection of raw intensity data at several points on the peak. The diffracted intensity (x-rays counted per unit time) or inverse intensity (time for a fixed number of x-rays to be counted) is determined to a precision exceeding 1% at several fixed diffraction

angles, 2θ , spanning the diffraction peak. Depending on the method to be used for peak location, 3 to 15 individual data points and 2 background points are measured using standard diffractometer techniques. If data are collected using a position-sensitive detector, the diffracted intensity can be determined at dozens of data points spanning the diffraction peak. Sharp diffraction peaks, such as those shown in curve A in Fig. 5, may be located using intensity data of lower precision than that required for broad peaks, as shown in curve D. The number of x-rays to be collected, and therefore the time required for stress measurement to a fixed precision, increases as the diffraction peaks broaden.

Before determining a diffraction-peak position, the raw measured intensities must be corrected for Lorentz polarization and absorption. A sloping background intensity is then corrected by subtracting the background, assuming a linear variation beneath the diffraction peak. Various numerical methods are available to calculate the position of the diffraction peak. The simplest method, incorporated in early automated diffraction equipment, is to locate 2θ positions on either side of the peak at which the intensity is equal and assume the peak position to be at the midpoint. A straight line can be fitted to the opposing sides of the diffraction peak and the point of intersection of the two lines taken as a peak position (Ref 10). Early SAE literature recommends calculating the vertex of the parabola defined by three points confined to the top 15% of the peak (Ref 11). A significant improvement in precision can be achieved, approaching the 0.01° resolution of most diffractometers, by collecting 5 to 15 data points in the top 15% and fitting a parabola by least squares regression before calculation of the peak vertex.

If the intensity is measured at many points ranging across the entire $K\alpha$ doublet, the peak position can be calculated as the centroid of the area above the background or by autocorrelation. Both of these area-integration methods are independent of the peak shape, but are extremely sensitive to the precision with which the tails of the diffraction peak can be determined.

All the above methods are effective, regression fit parabola being superior, if applied to a single symmetrical diffraction peak profile, such as the simple $K\alpha_1$ peak shown in curve A in Fig. 5 or the fully combined doublet shown in curve D. All can lead to significant error in the event of partial separation of the doublet, as shown in curve B (Fig. 5). Partial separation commonly results from defocusing as the sample is tilted through a range of ψ angles. If residual stresses are measured as a function of depth, diffraction peaks can vary from breadths similar to curve D (Fig. 5) at the cold-worked surface through a continuous range of blending to complete separation beneath the cold-work layer, as shown in curve A. All the techniques of peak location discussed can lead to

significant error in stress measurement as the degree of doublet separation varies.

The Rachinger correction (Ref 12) can be applied to separate the $K\alpha$ doublet before fitting parabolas, but the precision of the correction diminishes on the $K\alpha_2$ side of the combined profile and is generally inadequate for precise residual stress measurement. Fitting Pearson VII distribution functions (Cauchy to Gaussian bell-shaped, as described in Ref 13 and 14) separately to the $K\alpha_1$ and $K\alpha_2$ diffraction peaks, assuming a doublet separation based on the difference in wavelength, provides a method of peak location that overcomes most of the problems outlined above.

Figures 6 and 7 show the effect of the peak-location method on the results obtained. Figure 6 illustrates comparison of the same data reduced using Pearson VII distribution functions and a five-point least squares parabolic fit for ground Ti-6Al-4V using the (21.3) planes for residual stress measurement. Apparent nonlinearities in d versus $\sin^2\psi$ for the parabola fit are due to inaccurate diffraction-peak location in the presence of partial blending of the $K\alpha$ doublet. Figure 7 shows the errors in stress measurement by the two methods of peak location applied to the identical data for the entire stress profile. The errors for the distribution function fit are smaller than the plotting symbols at all depths.

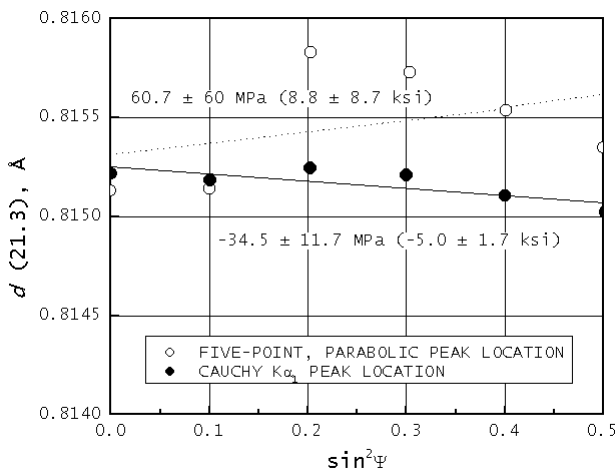


Fig. 6 Comparison of $d(21.3)$ versus $\sin^2\psi$ data taken 0.176 mm (0.0069 in.) below the surface for a ground Ti-6Al-4V sample using two diffraction peak location methods

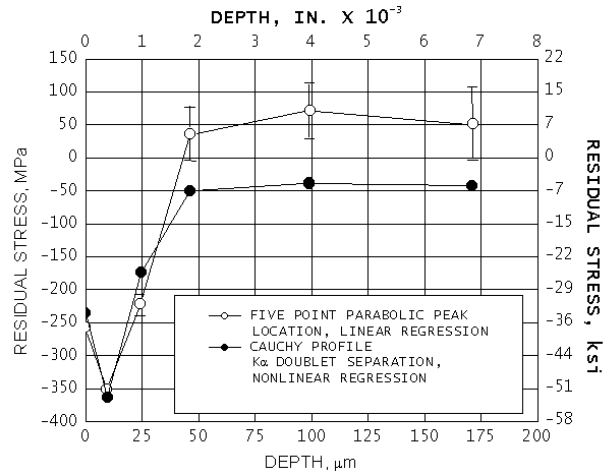


Fig. 7 -Comparison of residual stress patterns derived using Cauchy and parabolic peak location for a ground Ti-6Al-4V sample using a six-angle $\sin^2\psi$ technique. Errors in stress measurement by two methods of diffraction-peak location are shown.

Microstress Determination and line Broadening.

Diffraction peak broadening caused by microstresses in the crystal lattice can be separated into components due to strain in the crystal lattice and crystallite size. Separation of the broadening, which is of instrumental origin, from that due to lattice strain and crystallite size is performed using Fourier analysis of the diffraction-peak profile and data collection sufficient to define precisely the shape of the entire diffraction peak. Analysis of the Fourier series terms allows separation of the components of the broadening attributable to lattice strain from that caused by reduction in the crystallite size. However, this method requires extensive data collection and depends on the precision with which the tails of the diffraction peak can be separated from the background intensity.

For most routine analyses of microstresses associated with cold working or heat treatment for which separation of the strain and size components is not necessary, much simpler determinations of diffraction-peak breadth are adequate. The diffraction-peak width can be quantified precisely as the integral breadth (total area under the peak divided by diffraction-peak height) or the width at half the height of the diffraction peak. The width of the diffraction peak can be measured directly from strip-chart recordings or calculated from the width of the function fitted to the diffraction-peak profile during macrostress measurement. Microstresses and macrostresses can then be determined simultaneously from the peak breadth and position.

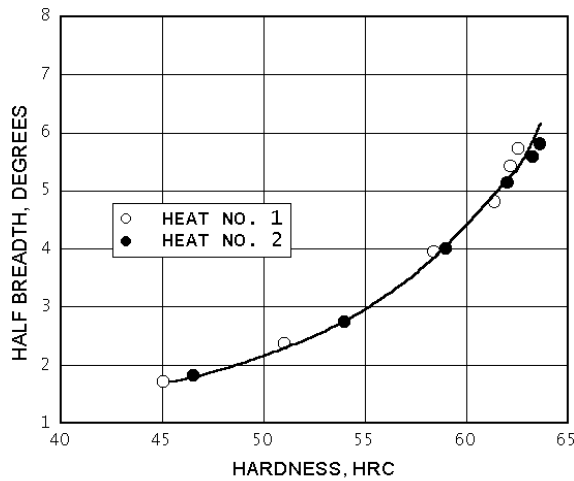


Fig. 8 -Diffraction-peak breadth at half height for the (211) peak for M50 high-speed tool steel as a function of Rockwell hardness.

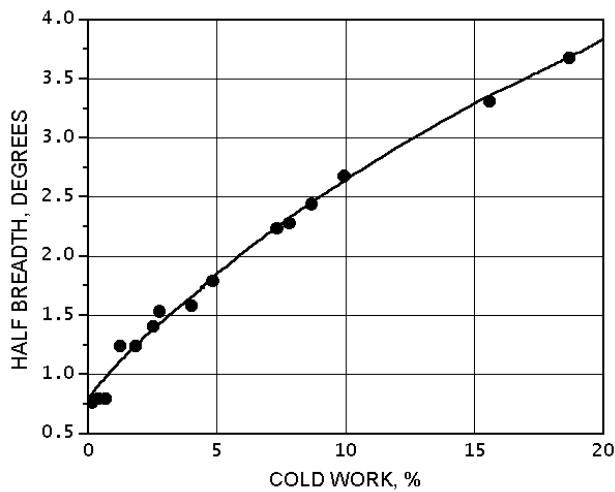


Fig. 9 -Diffraction-peak breadth at half height for the (420) peak for Rene 95 as a function of cold-working percentage

Figures 8 and 9 show empirical relationships established between diffraction-peak breadth at half height for the (211) peak for M50 high-speed tool steel as a function of hardness and for the (420) peak breadth as a function of percent cold work for Rene 95, respectively. These empirical curves can be used to calculate the hardness or cold work in conjunction with macroscopic residual stress measurement. For the preparation of the hardness curve, a series of coupons are quenched and tempered to known hardness. The peak breadth is then measured using the same slit system and peak-location method used for macrostress measurement. For the percent cold work curve, samples are heat treated, then pulled in tension to produce a series of coupons with various known amounts of cold work. Because the initial heat treatment may alter significantly the initial peak breadth before cold work, the coupons must receive the same heat treatment as the samples to be measured before inducing known amounts of cold work.

Sample fluorescence complicates the selection of radiation to be used for residual stress measurement. The radiation necessary for the highest precision techniques may cause fluorescence of the elements present in the sample under investigation. The use of Cu K α radiation for residual stress measurement in alloys containing iron, chromium, or titanium can result in fluorescent background intensities many times as intense as the diffracted radiation, greatly reducing the signal-to-noise ratio. Problems with fluorescence may be overcome in some cases by use of metal foil filters, but generally require use of a crystal monochromator or high energy resolution solid-state detector. Failure to eliminate fluorescence can degrade severely the precision with which the diffraction peak can be located accurately, increasing random experimental error significantly. Diffracted beam monochromators and solid-state detectors can be used only on standard laboratory diffractometers. The position-sensitive detectors available for residual stress measurement are the gas-filled proportional counter or fluorescence screen type and have insufficient energy resolution to overcome fluorescence.

SOURCES OF ERROR

Instrumental and Positioning Errors. The principal sources of error in x-ray diffraction residual stress measurement are related to the high precision with which the diffraction-peak position must be located. Errors of approximately 0.025 mm (0.001 in.) in alignment of the diffraction apparatus or positioning of the sample result in errors in stress measurement of approximately 14 MPa (2 ksi) for high diffraction angle techniques and increase rapidly as the diffraction angle is reduced.

Instrument alignment requires coincidence of the θ and ψ axes of rotation and positioning of the sample such that the diffracting volume is centered on these coincident axes. If a focusing diffractometer is used, the receiving slit must move along a true radial line centered on the axes of rotation. All these features of alignment can be checked readily using a stress-free powder sample (Ref 15). If the diffraction apparatus is properly aligned for residual stress measurement, a loosely compacted powder sample producing diffraction at approximately the Bragg angle to be used for residual stress measurement should indicate not more than ± 14 MPa (± 2 ksi) apparent stress. Alignment and positioning errors result in systematic additive error in residual stress measurement.

Effect of Sample Geometry. Excessive sample surface roughness or pitting, curvature of the surface within the irradiated area, or interference of the sample geometry with the diffracted x-ray beam can result in systematic error similar to sample displacement. Coarse grain size, often encountered in cast materials, can lessen the number of crystals contributing to the diffraction peak such that the peaks become asymmetrical, resulting in random error

in diffraction-peak location and residual stress measurement. Rocking of coarse-grained samples about the ψ axis through a range of a few degrees during measurement can be used to increase the number of crystals contributing to the diffraction peak in coarse-grained samples to allow residual stress measurement on samples with a grain size as large as ASTM No. 1 (Ref 16). Residual stress generally cannot be measured reliably using x-ray diffraction in samples with coarser grain sizes.

X-Ray Elastic Constants. A major source of potential systematic proportional error arises in determination of the x-ray elastic constants $(E/1 + \nu)_{(hkl)}$. The residual stress measured is proportional to the value of the x-ray elastic constants, which may differ by as much as 40% from the bulk value due to elastic anisotropy. The x-ray elastic constant must be determined empirically by loading a sample of the material to known stress levels and measuring the change in the lattice spacing as a function of applied stress and ψ tilt (Ref 17). The x-ray elastic constant can then be calculated from the slope of a line fitted by least squares regression through the plot of the change in lattice spacing for the ψ tilt used function of applied stress.

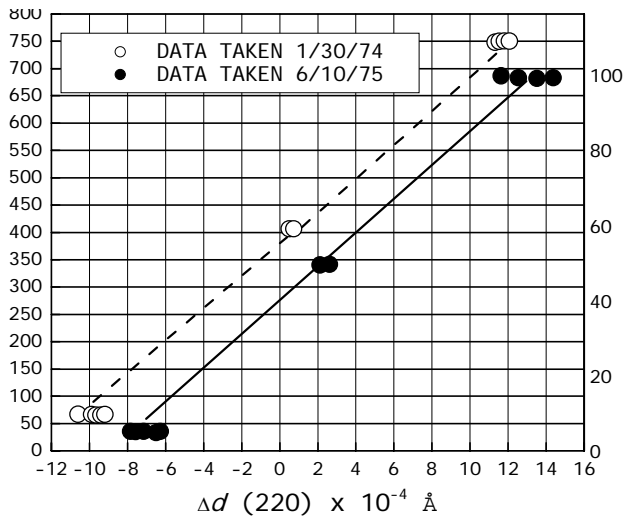


Fig. 10 -X-ray elastic constant determination for Inconel 718, (220) planes $\Delta\psi = 45^\circ$ $d_0 = 1.1272 \text{ \AA}$

Figure 10 shows data obtained for determination of the x-ray elastic constants in Inconel 718. With instrumented samples placed in four-point bending, the x-ray elastic constant can typically be determined to an accuracy of $\pm 1\%$. Table 1 lists elastic constants determined in four-point bending for various alloys along with the bulk elastic constants and the potential systematic proportional error that could result from use of the bulk values. X-ray elastic constants should be determined whenever possible to minimize systematic proportional error.

SUBSURFACE MEASUREMENT AND REQUIRED CORRECTIONS

Measuring residual stress distributions as functions of depth into the sample surface necessitates electropolishing layers of material to expose the subsurface layers. Electropolishing is preferred for layer removal because no residual stresses are induced, and if properly performed, preferential etching of the grain boundaries does not occur. Any mechanical method of removal, regardless of how fine the abrasive or machining method, deforms the surface and induces residual stresses, altering severely the state of stress present in the sample. Such methods must be avoided. Thick layers can be removed using a combined machining or grinding procedure, followed by electropolishing to remove at least 0.2 mm (0.008 in.) of material to eliminate the machining or grinding residual stresses.

Subsurface Stress Gradients. Although the x-ray beam penetrates only to shallow depths (approximately 0.005 mm, or 0.0002 in.) beneath the exposed surface, the residual stress distributions produced by machining and grinding may vary significantly over depths of this order. Because the x-ray beam is attenuated exponentially as it passes into and out of the sample, stress measurements conducted in the presence of such a subsurface stress gradient yield an exponentially weighted average of the stress at the exposed surface and in the layers below. The intensity of the radiation penetrating to a depth x is:

$$I(x) = I_0 e^{-\mu x}$$

where I_0 is the initial intensity, μ is the linear absorption coefficient, and e is the natural logarithm base (2.71828...). If the linear absorption coefficient is known, this exponential weighting can be unfolded provided measurements have been conducted at sufficient number of closely spaced depths to define the stress gradient adequately. Correction for penetration of the radiation into the subsurface stress gradient requires calculating the derivative of the lattice spacing at each ψ tilt as a function of depth. The linear absorption coefficient is calculated from the chemical composition, mass absorption coefficients for the elemental constituents of the alloy, density of the alloy, and radiation used. Failure to correct for penetration of the radiation into the stress gradient can lead to errors as large as 345 MPa (50 ksi).

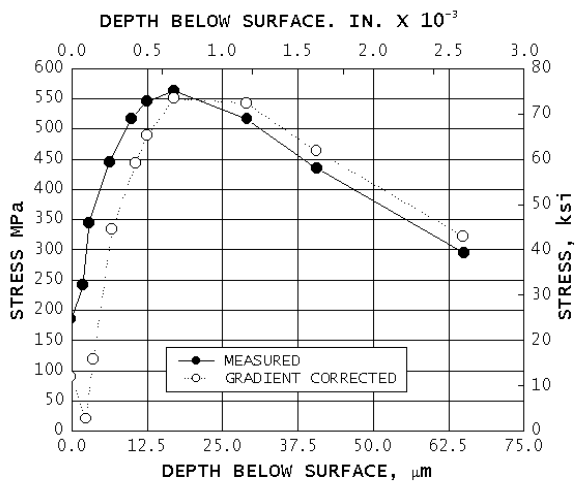


Fig. 11 – Effect of the stress gradient correction on the measurement of near-surface stresses for ground 4340 steel, 50 HRC

Figure 11 shows an example of the effect of the correction on the residual stress profile produced in ground 4340 steel. Errors due to the subsurface stress gradient are generally maximum at the surface of the sample and become minimal beneath the highly deformed surface layer. Nondestructive surface residual stress measurements are subject to significant error on machined or ground surfaces due to the presence of the subsurface stress gradient.

Significant relaxation of stress in the surface exposed by layer removal can occur in determination of subsurface residual stresses. If the sample geometry and nature of the residual stress distribution conform to the simple symmetries of flat plates or cylindrical bodies, closed-form solutions are available to correct the results obtained on the surfaces exposed by electropolishing for removal of the stressed layers above (Ref 18). These corrections involve integration over the residual stress measured in the layers removed from the exposed layer back to the original surface. The accuracy of these corrections depends on the depth resolution with which the stress distribution is measured. Correction for layer removal can be combined with correction for sectioning to determine the total state of residual stress before dissection of the sample.

The magnitude of the layer-removal stress-relaxation correction, which depends on the stress in the layers removed and the sample geometry, increases with the total strain energy released. For massive samples from which only thin layers have been removed or for any sample geometry in which no significant stresses are present, correction will be insignificant. However, the correction can be large for some combinations of stress distribution and geometry. Figure 12 shows the longitudinal residual stress distribution with and without

correction for complete removal of the carburized case on 16-mm (5/8-in.) diam steel shaft.

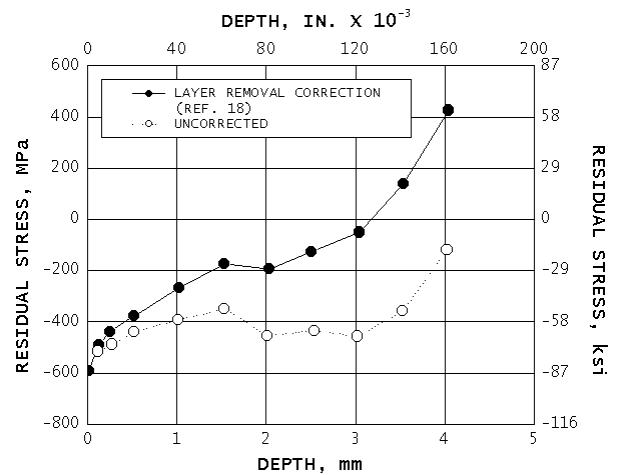


Fig. 12 -Longitudinal residual stress distribution with and without correction for removal of the carburized case from a 16-mm (5/8-in.) diam 1070 steel shaft

Many components, such as gear teeth and turbine blades, do not conform to the simple geometries and assumed stress fields to which the closed-form layer-removal corrections apply. For these geometries, electropolishing in a confined pocket to minimize stress relaxation, which is assumed to be negligible, is the only practical approach.

APPLICATIONS

The following examples result from investigations performed on horizontal laboratory diffractometers modified for stress measurement and instrumented with a lithium-doped silicon solid-state detector for suppression of sample fluorescence. The examples implement the two-angle technique and the fitting of a parabola to the top 15% or a Cauchy profile of the entire diffraction peak, as appropriate for the symmetry of the diffraction peaks produced. Results were corrected for Lorentz polarization and absorption as well as a sloping background intensity. Subsurface results were corrected for penetration of the radiation into the subsurface stress gradient and for sectioning and layer removal stress relaxation, as appropriate.

The elastic constants used to calculate macroscopic stress from strain in the crystal lattice were obtained empirically by loading an instrumented beam of the alloy under investigation in four-point bending. The samples were positioned to the center of the diffractometer using a feeler gage capable of repeat positioning precision of ±0.05 mm (±0.002 in.). The alignment of the diffractometers was established and checked using nickel or iron powder in accordance with ASTM E 915 (Ref 15).

Example 1: Subsurface Residual Stress and Hardness Distributions in an Induction-Hardened Steel Shaft.

The longitudinal residual stress and hardness distributions through the case produced by induction hardening of a 1070 carbon steel shaft were investigated to qualify a modification of the induction-hardening procedure. The sample consisted of a nominally 205-mm (8-in.) long shaft of complex geometry; a 16-mm (5/8-in.) diam. induction hardened bearing surface was the region of interest.

The sample was first sectioned to approximately 100 mm (4 in.) in length to facilitate positioning on the diffractometer. Because the sample was cut a distance of several diameters from the area of interest, no attempt was made to monitor sectioning stress relaxation, assumed to be negligible. X-ray diffraction macroscopic residual stress measurements were performed using the two angle Cr K α (211) technique in the longitudinal direction as a function of depth to approximately 4 mm (0.16 in.) beneath the original surface, fully removing the hardened case. The material was removed by electropolishing complete cylindrical shells as necessary to correct for layer removal stress relaxation using closed-form solutions (Ref 18). Simultaneous determinations of the breadth of the Cauchy diffraction-peak profile fitted to the K α_1 peak were used to calculate the hardness of the material using an empirical relationship similar to that shown in Fig. 8, which was previously established for 1070 steel.

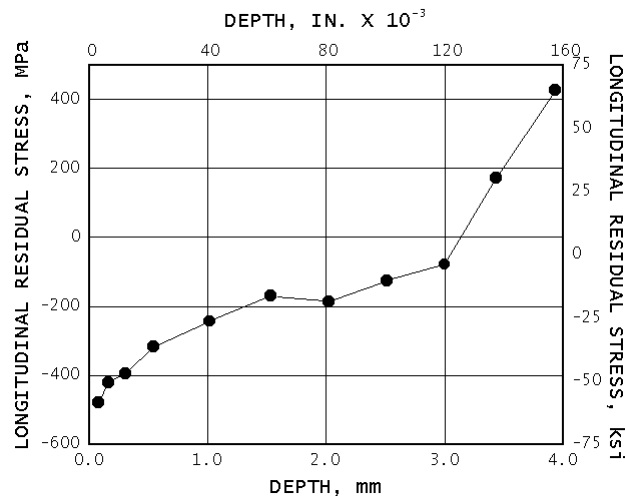


Fig. 13 -Longitudinal residual stress distribution in an induction-hardened 1070 carbon steel shaft

Figure 13 shows the longitudinal residual stress distribution corrected for penetration of the radiation into the stress gradient, essentially negligible for the gradual stress gradient produced by induction hardening, and for layer removal, which builds to corrections as large 550 MPa (80 ksi) at the maximum depth. The fully corrected results show surface compression of approximately -550

MPa (-80 ksi) diminishing initially in a near-exponential fashion, then more gradually beyond depths of approximately 1.5 mm (0.060 in.). The stress distribution crosses into tension at a nominal depth of 3 mm (0.125 in.) and rises to relatively high tension in the core of the shaft, approaching 517 MPa (75 ksi) at the maximum depth of 4 mm (0.160 in.) examined.

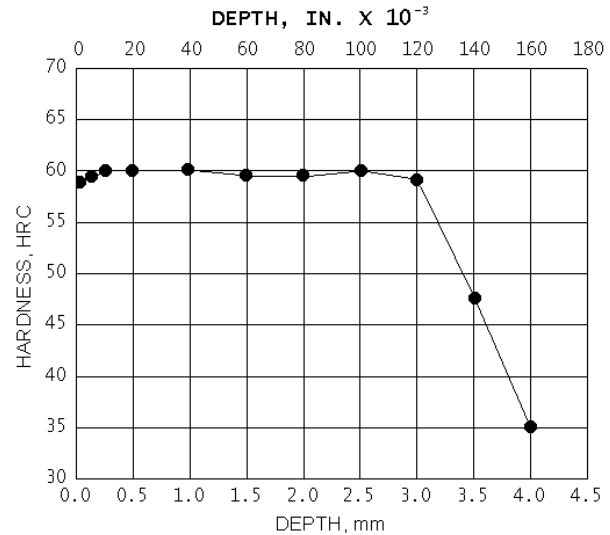


Fig. 14 -Hardness (Rockwell C scale) distribution in an induction-hardened 1070 carbon steel shaft

Figure 14 illustrates the hardness distribution calculated from the breadth of the (211) diffraction –peak profile fitted using Cauchy distribution function to separate the K α doublet. The hardness was found to be extremely uniform, varying between 59 and 60 HRC to a depth of 3 mm (0.120 in.). At approximately the depth at which the longitudinal residual stress distribution goes into tension, the hardness begins to diminish linearly, dropping to approximately 35 HRC at the maximum depth examined in the core of the shaft.

Example 2: Residual Stress and Percent Cold Work Distribution in Belt Polished and Formed Inconel 600 tubing.

Inconel 600 tubing of the type used for steam generators subject to potential stress corrosion cracking is fabricated by cross roll straightening and belt polishing of the outer diameter surface. Belt polishing induces subsurface residual stress and cold-work distributions, which can impact on the state of residual stress present in the tubing when it is formed into U-bends.

A single sample of mill-annealed and belt-polished straight tubing was investigated to determine the longitudinal subsurface residual stress and percent plastic strain distribution as functions of depth produced by belt polishing. X-ray diffraction macro and microstress measurements were performed using a Cu K α (420) two-angle technique. The K α_1 diffraction peak was separated

from the doublet by fitting a Cauchy diffraction-peak profile. The X-ray elastic constant required had been determined previously by loading a sample of the alloy in four-point bending. An empirical relationship was established by annealing, then drawing samples of tubing to plastic strain levels in excess of 20%, generating an empirical relationship similar to that shown in Fig. 9.

The subsurface longitudinal residual stress and percent plastic strain distributions were determined by electropolishing thin layers of material in complete cylindrical shells from around the circumference of the 16-mm (0.625-in.) nominal diameter tubing. Layer removal began with 0.005-mm (0.0002-in.) thick layers near the sample surface, the increment between layers increasing with depth to nominally 0.4 mm (0.017 in.) beneath the original surface. Corrections were applied for the stress gradient and layer removal.

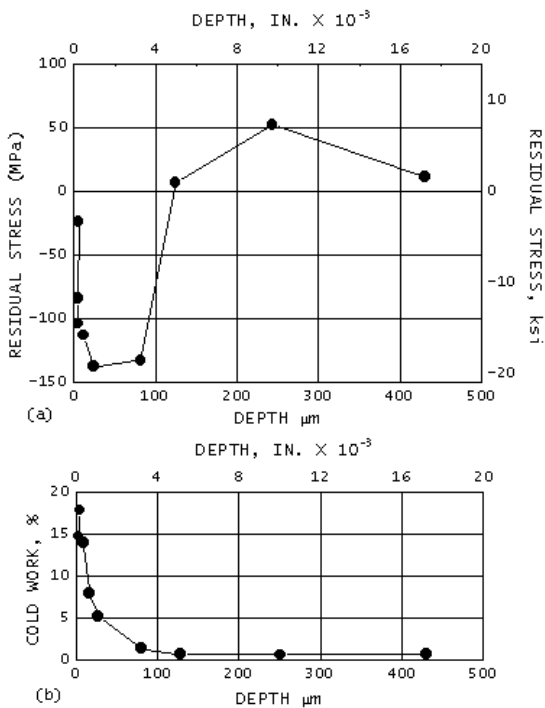


Fig. 15 – Longitudinal residual stress and percent cold work distributions in belt-polished Inconel 600 tubing.

Figure 15 illustrates the results of the longitudinal residual stress and percent plastic strain distributions. The residual stress distribution shows a pronounced gradient from approximately -35 MPa (-5 ksi) at the surface to a maximum compressive value of approximately -150 MPa (-20 ksi) at a nominal depth of 0.05 mm (0.002 in.). With increasing depth, the stress distribution rises back into tension at approximately 0.13 mm (0.005 in.), with a low-magnitude tensile profile peaking at nominally 55 MPa (8 ksi) at greater depths. The plastic strain distribution shows a slight hook near the surface of the sample; the percent cold work approaches 19% at a nominal depth of 5 mm (0.0002 in.). With increasing depth, the cold-work

distribution decreases nearly exponentially to negligible values beyond approximately 0.13 mm (0.005 in.) beneath the belt-polished surface.

A 63-mm (2.5-in.) U-bend manufactured from Inconel 600 tubing was strain gaged at the apex and sectioned to remove approximately a 50 mm (2 in.) arc length. This portion of the U-bend was mounted in a special fixture providing precision orientation around the circumference of the tubing to an accuracy of 0.1°. X-ray diffraction residual macrostress measurements were made on the existing surface as a function of angle θ around the circumference of the tubing.

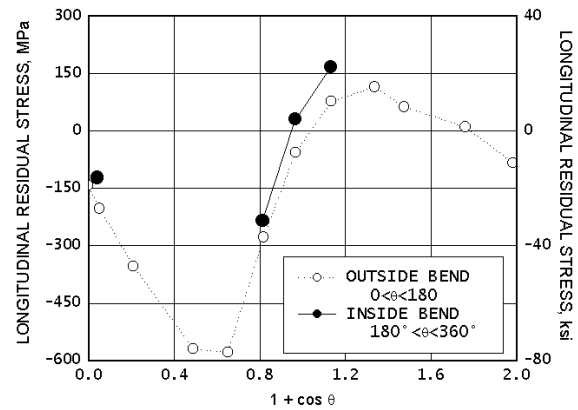


Fig. 16 -Longitudinal residual stress as a function of the quantity $(1 + \cos \theta)$ for a 63-mm (2.5-in.) Inconel 600 U-bend

Figure 16 shows the results of these measurements; the longitudinal surface residual stress has been plotted as a function of the quantity $(1 + \cos \theta)$ to expand the central portion of the plot, at which the sharp transition occurs between maximum compression and tension. The position around the circumference of the tubing ranges from the outside of the bend at the origin around the flank, or neutral axis, at $1(1 + \cos \theta)$ and around to the inside of the bend. The results shown as open circles indicate the longitudinal residual stress around one side of the tubing; closed circles, comparable measurements made on the opposing side.

The x-ray beam was limited to a height of 0.5 mm (0.020 in.) and a width of 2.5 mm (0.1 in.) along the axis of the tubing. The small beam size was necessary to optimize spatial resolution in the presence of the pronounced stress gradient occurring on the flank of the tubing. The compressive stresses produced around the outside of the bend exceed -550 MPa (-80 ksi) in a material with a nominal annealed yield strength of 240 MPa (35 ksi). The presence of these high stresses after forming result from cold working at the tubing induced during belt polishing. Cold working of Inconel 600 to 20% increases yield strength to approximately 690 MPa (100 ksi). Cold-worked surface layers in components subjected to

subsequent forming frequently result in complex residual stress distributions having magnitudes often exceeding the yield strength of the undeformed material.

Example 3: Local Variations in Residual Stress Produced by Surface Grinding. The high spatial resolution of x-ray diffraction residual stress measurement was applied to determine the longitudinal surface and subsurface residual stress variation near grinder bums produced by traverse grinding of a sample of 4340 steel with a hardness of 50 HRC. Three samples were initially investigated: two were ground abusively to produce grinder burn, and one was ground gently using adequate coolant. X-ray diffraction residual stress measurements were performed initially on only the surfaces of the three samples using a Cr K α (211) two-angle technique. The diffraction-peak positions were located using a five-point parabolic regression procedure, assuming the K α doublet to be completely blended into a single symmetrical peak for all measurements performed in the hardened material. The irradiated area was 0.5 by 6.4 mm (0.020 by 0.250 in), with the long axis aligned in the grinding direction. Measurements were conducted using the narrow irradiated area as a function of distance across the surface of each sample. A single measurement using a 12.5-by 6.4-mm (0.5- by 0.250-in.) irradiated area spanning nearly the entire region covered by the series of measurements made with the smaller irradiated zone was then performed on each sample.

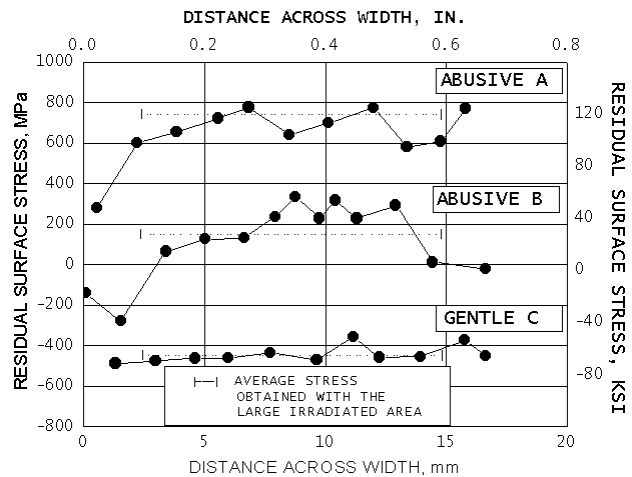


Fig. 17 – Variations in longitudinal surface residual stress produced by surface grinding 4340 alloy steel (50 HRC) samples

Figure 17 shows the results of the surface measurements. The individual measurements made using the 0.5-mm (0.02-in.) wide irradiated area are shown as open circles. The single result obtained using the 13-mm (0.5-in.) wide beam is plotted as a dashed line; the bounds on the line indicate the approximate extent of the large irradiated area. The gently ground sample was found to be uniformly in compression, with surface stresses ranging from approximately -400 to -520 MPa (-60 to -75 ksi) at

all points examined. The abusively ground sample A was found to be entirely in tension; the values range from 275 to 825 MPa (40 to 120 ksi) across the width of the sample. Abusively ground sample B shows regions of compression and tension, with visible grinder burn associated with the tensile peaks occurring above approximately 275 MPa (40 ksi) near the center of the sample. The results for the large irradiated area provide nominally the arithmetic average of the small area results.

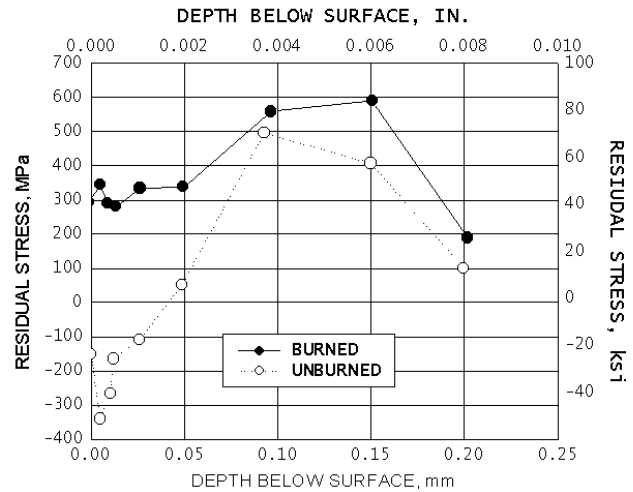


Fig. 18 – Subsurface residual stress profiles produced in burned and unburned regions of abusively ground 4340 alloy steel (50 HRC)

The subsurface residual stress distribution was then determined at the point of maximum compression and maximum tension on the abusively ground sample B using the 0.5-mm (0.020-in.) irradiated area. The sample was electropolished completely across the width as measurements were conducted at the two locations of interest. The subsurface results shown in Fig. 18 indicate compressive stresses near the edge of the unburned sample at the point of maximum compression that extend to a nominal depth of 0.05 mm (0.002 in.) and rise into tension approaching 500 MPa (70 ksi) at greater depths. The burned region shows entirely tensile stresses ranging from approximately 275 to 345 MPa (40 to 50 ksi) to a depth of 0.05 mm (0.002 in); it rises into tension approximately 600 MPa (90 ksi) further below the surface.

The residual stresses produced by many grinding and machining operations can vary significantly over local distances, particularly if there is significant heat input, loss of coolant, or tool dulling. Further, use of a nondestructive surface measurement of residual stress or a nital etch to reveal grinder burn may not reveal subsurface tensile residual stresses that could degrade fatigue performance severely

Example 4: Longitudinal Residual Stress Distribution in Welded Railroad Rail. Continuously welded railroad

rail may be subject to high tensile or compressive applied stresses resulting from thermal contraction and expansion in the field. The presence of significant residual stresses in the flash butt welded joints of such rail could contribute to failure near the welds.

To determine the longitudinal residual stresses in the hardened head of welded rail near the weld, a nominally 200 mm (8 in.) portion of rail containing the weld was band sawed from a section of continuous rail after welding. Sectioning stress relaxation was assumed to be negligible.

The surface of the rail head was prepared by electropolishing to a nominal depth of 0.25 mm (0.010 in.) to remove any surface residual stresses that may have originated from sources other than welding. X-ray diffraction longitudinal residual stress measurements were then conducted using the two angle technique at a series of positions across the center line of the weld, which was located by etching with nital before electropolishing. A Cr K α (211) technique was used, locating the diffraction peak using a parabolic regression procedure. The rail head was induction hardened, and the K α doublet was completely blended and symmetrical throughout the hardened head portion of the rail.

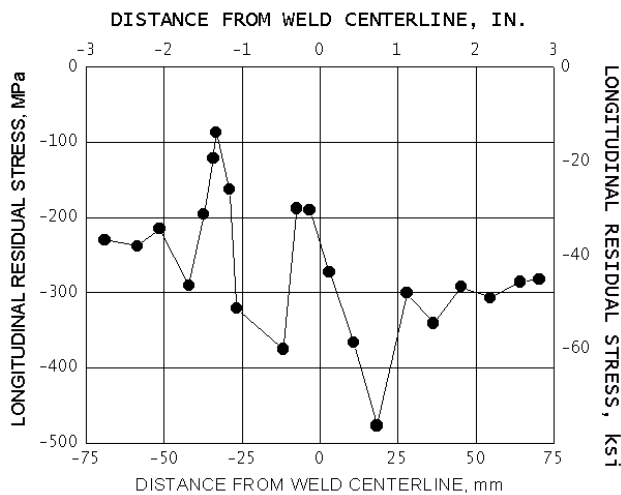


Fig. 19 – Longitudinal residual stress distribution across a flash butt welded induction-hardened railroad rail head.

Figure 19 illustrates the results of the longitudinal measurements, which reveal an entirely compressive longitudinal residual stress distribution at the top of the head of the rail near the weld and an asymmetrical

oscillating pattern of residual stress different from that which would have been predicted by analytical solution. The results of repeat measurements confirmed the nature of the stress distribution.

The analytical methods for predicting the residual stresses produced by welding generally predict a symmetrical residual stress distribution around the weld fusion line; however, the actual stress distributions revealed by measurement are often substantially more complex than those predicted.

Example 5: Determination of the Magnitude and Direction of the Maximum Residual Stress Produced by Machining. The direction of maximum residual stress, that is, most tensile or least compressive, is assumed to occur in the cutting or grinding direction during most machining operations. This is frequently the case, but the maximum stress often occurs at significant angles to the cutting direction. Furthermore, the residual stress distributions produced by many cutting operations, such as turning, may be highly eccentric, producing a highly tensile maximum stress and a highly compressive minimum stress.

The residual stress field at a point, assuming a condition of plane stress, can be described by the minimum and maximum normal principal residual stresses, the maximum shear stress, and the orientation of the maximum stress relative to some reference direction. The minimum stress is always perpendicular to the maximum. The maximum and minimum normal residual stresses, shown as σ_1 and σ_2 in Fig. 2, and their orientation relative to a reference direction can be calculated along with the maximum shear stress using Mohr's circle for stress if the stress σ_ϕ is determined for three different values of ϕ .

To investigate the minimum and maximum normal residual stresses and their orientation produced by turning an Inconel 718 cylinder, x-ray diffraction residual stress measurements were performed in the longitudinal, 45°, and circumferential directions at the surface and at subsurface layers to a nominal depth of 0.1 mm (0.004 in.), exposing the subsurface depths by electropolishing complete cylindrical shells around the cylinder. The cylinder was nominally 19 mm (0.75 in.) in diameter and uniformly turned along a length of several inches. The irradiated area was limited to a nominal height of 1 mm (0.05 in.) around the circumference by 2.5 mm (0.10 in.) along the length. Measurements were conducted using a Cu K α (420) two-angle technique, separating the K α_1 peak from the doublet using a Cauchy peak profile.

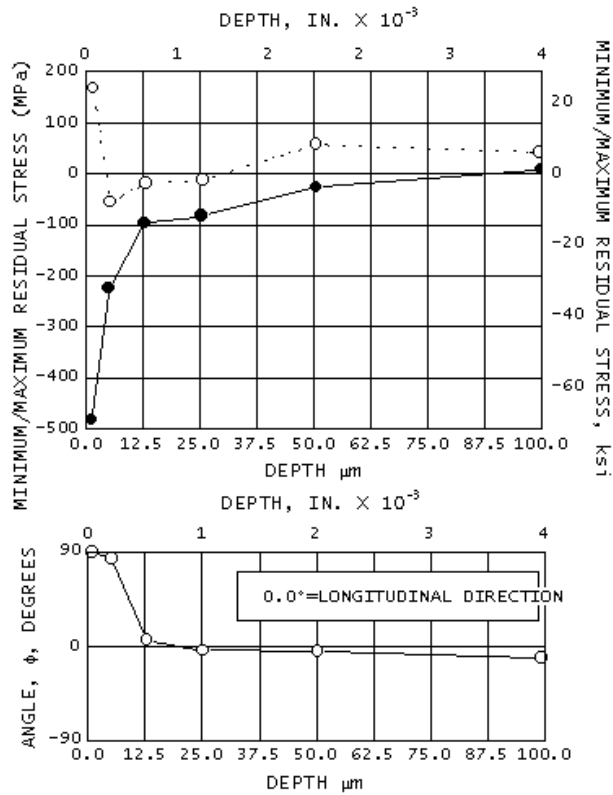


Fig. 20 Minimum and maximum principal residual stress profiles and their orientation relative to the longitudinal direction in a turned Inconel 718 cylinder

The measurements performed independently in the three directions were combined using Mohr's circle for stress at each depth to calculate the minimum and maximum normal residual stresses and their orientation defined by the angle ϕ , which was taken to be a positive angle counterclockwise from the longitudinal axis of the cylinder. Figure 20 illustrates the results, showing the maximum and minimum principal residual stress profiles and their orientation relative to the longitudinal direction. The maximum stresses are tensile at the surface, in excess of 140 MPa (20 ksi), dropping rapidly into compression at a nominal depth of 0.005 mm (0.0002 in.). The maximum stress returns into tension at depths exceeding 0.025 mm (0.001 in.) and remains in slight tension to the maximum depth of 0.1 mm (0.004 in.) examined. The minimum residual stress is in compression in excess of -480 MPa (-70 ksi) at the turned surface and diminishes rapidly in magnitude with depth to less than -138 MPa (-20 ksi) at a depth of 0.013mm (0.0005 in.). The minimum stress remains slightly compressive and crosses into tension only at the maximum depth examined. The orientation of the maximum stresses is almost exact in the circumferential direction (90° from the longitudinal) for the first two depths examined. For depths of 0.013 mm (0.0005 in.) to the maximum depth of 0.1 mm (0.004 in.), the maximum stress is within approximately 10° of the longitudinal direction.

The results appear to indicate that stresses within approximately 0.013 mm (0.0005 in.) of the sample surface are dominated by machining, which resulted in a maximum stress direction essentially parallel to the cutting action. At greater depths, the stress distribution may be governed not by the machining as much as by stresses that may have been present due to forging or heat treatment.

REFERENCES

1. M.E. Hilley, Ed., *Residual Stress Measurement by X-Ray Diffraction*, SAE J784a, Society of Automotive Engineers, Warrendale, PA, 1971, p 21-24
2. B.D. Cullity, *Elements of X-Ray Diffraction*, Addison Wesley, 2nd ed., 1978, p 470
3. M.E. Hilley, Ed., *Residual Stress Measurement by X-Ray Diffraction*, SAE J784a, Society of Automotive Engineers, Warrendale, PA, 1971, p 19
4. M.E. Hilley, Ed., *Residual Stress Measurement by X-Ray Diffraction*, SAE J784a, Society of Automotive Engineers, Warrendale, PA, 1971, p 20
5. R.H. Marion and J.B. Cohen, *Adv. X-Ray Anal.*, Vol 18, 1975, p 466
6. P.S. Prevéy, *Adv. X-Ray Anal Vol 19*, 1976, p 709
7. H. Dölle and J.B. Cohen, *Met. Trans.*, Vol 11A, 1980, p 159
8. H. Dölle, *J. Appl. Cryst.*, Vol 12, 1979, p 498
9. M.E. Hilley, Ed., *Residual Stress Measurement by X-Ray Diffraction*, SAE J784a, Society of Automotive Engineers, Warrendale, PA, 1971, p 61
10. A.L. Christenson and E.S. Rowland, *Trans. ASM*, Vol 45, 1953, p 638
11. D.P. Koistinen and R.E. Marburger, *Trans. ASM*, Vol 51, 1959, p 537
12. W.A. Rachinger, *J. Sci. Instr.*, Vol 25, 1948, p 254
13. S.K. Gupta and B.D. Cullity, *Adv. X-Ray Anal.*, Vol 23, 1980, p 333
14. P.S. Prevéy, *Adv. X-Ray Anal.*, Vol 29, to be published
15. "Standard Method for Verifying the Alignment of X-ray Diffraction Instrumentation for Residual Stress Measurement," E 915, *Annual Book of ASTM Standards*, Vol 03.01, ASTM, Philadelphia, 1984, p 809-812
16. "Standard Methods for Determining Average Grain Size," E 112, *Annual Book of ASTM Standards*, Vol 02.01, ASTM, Philadelphia, 1984, p 1073-1107
17. P.S. Prevéy, *Adv. X-Ray Anal.*, Vol 20, 1977, p 345
18. M.G. Moore and W.P. Evans, *Trans. SAE*, Vol 66, 1958, p 340